RBRH

Revista Brasileira de Recursos Hídricos
Brazilian Journal of Water Resources
Versão On-line ISSN 2318-0331
RBRH, Porto Alegre, v. 26, e9, 2021
Scientific/Technical Article

https://doi.org/10.1590/2318-0331.262120200161

Effects of return periods on flood hazard mapping: an analysis of the UFSC Campus Basin, Florianópolis city, Brazil

Efeito dos períodos de retorno no mapeamento de perigo de inundação: uma análise da Bacia do Campus da UFSC, Florianópolis, Brasil

Leonardo Romero Monteiro[1], Camyla Innocente dos Santos[2], Masato Kobiyama[3], Cláudia Weber Corseuil[4] & Pedro Luiz Borges Chaffe[2]

[1]Universidade do Estado de Santa Catarina, Joinville, SC, Brasil
[2]Universidade Federal de Santa Catarina, Florianópolis, SC, Brasil
[3]Universidade Federal do Rio Grande do Sul, Porto Alegre, RS, Brasil
[4]Universidade Federal de Santa Catarina, Araranguá, SC, Brasil

E-mails: leonardo.monteiro@udesc.br (LRM), camylainnocente@gmail.com (CIS), masato.kobiyama@ufrgs.br (MK), claudia.weber@ufsc.br (CWC), pedro.chaffe@ufsc.br (PLBC)

Received: November 03, 2020 - Revised: December 24, 2020 - Accepted: March 02, 2021

ABSTRACT

The development of urban areas exacerbates flood risk by increasing both runoff and the exposure of population and infrastructure. In this study, we highlight the importance of return period choice on flood hazard degree and flood hydraulics characteristics. We use the UFSC campus basin as a test bed and combine a hydrological and a hydrodynamic model to define the flood hazard intensity and flood hazard degree. Six hazard intensity maps were elaborated using different return periods (2, 10, 25, 50, 100 and 500-years) that characterize low and high recurrence scenarios. The low recurrence hazard map can be ideal to verify hazard effects on buildings, while the high recurrence hazard map helps to identify people security. All variables related to the rainfall effect and its consequences (e.g. rainfall intensity, flood mean velocity, and total flood area) follow a logarithmic relationship, with a small variation for higher return periods. We highlight how different return periods can influence flood hydraulics and flood hazard and should therefore be considered in flood hazard mapping.

Keywords: Flood hazard degree; Synthetic hyetograph; Return period.

RESUMO

O desenvolvimento de áreas urbanas intensifica o risco de inundação pelo acréscimo tanto do escoamento superficial quanto da exposição da população e infraestrutura. Neste trabalho, nós evidenciamos a importância da escolha do período de retorno para determinar o grau de perigo de inundação e suas características hidráulicas. A bacia do campus da UFSC foi utilizada para o teste, onde combinamos modelos hidrológicos e hidráulicos para definir a intensidade e grau de perigo de inundação. Seis mapas de intensidade de perigo foram elaborados a partir de diferentes períodos de retorno (2, 10, 25, 50, 100 e 500 anos), que foram usados para caracterizar cenários de baixa recorrência e alta recorrência. O mapa de baixa recorrência pode ser ideal para ver os efeitos nas construções enquanto o mapa de alta recorrência ajuda a identificar a segurança das pessoas. Observou-se que uma linha de tendência logarítmica se encaixa bem para todas as variáveis verificadas relacionadas a inundação (e.g. intensidade da chuva, velocidade média de inundação, área total de inundação). Este estudo é importante para compreender as diferenças entre os efeitos no mapeamento de perigo de inundação aos períodos de retorno e como podem influenciar as variáveis hidráulicas de inundação.

Palavras-chave: Grau de perigo de inundação; Hietograma sintético; Período de retorno.

This is an Open Access article distributed under the terms of the Creative Commons Attribution License, which permits unrestricted use, distribution, and reproduction in any medium, provided the original work is properly cited.

INTRODUCTION

Negative consequences of flood in society have been intensified in recent decades (Najibi & Devineni, 2018), which has lead most nations as well as the UN to execute various actions to reduce them. The development and concentration of population in urban areas intensify exposure and consequently increase the risk related to flood. Especially in developing countries like Brazil, inadequate urbanization or non-planned occupation of urban areas is one of the main factors that increases urban flood damages (Monteiro & Kobiyama, 2013; Speckhann et al., 2017).

Detailed flood hazard mapping is one alternative to improve management of the situation with increased exposure and vulnerability. A flood hazard map represents the spatial distribution of potential flood consequences which is a function of intensity and probability of flood occurrence. The flood intensity is related to the flow force that can untabify people, vehicles, and infrastructure. To map flood hazard areas with more details in terms of the flood intensity and frequency, the use of hazard indexes or category that consider water depth and velocity (e.g., Stephenson, 2002; Smith et al., 2014) are useful and practical.

Even that many different methods have been proposed, flood hazard mapping does not have a standard procedure that relates flow intensity and frequency. There are many factors that can influence flood hazard (Ball et al., 2019): velocity of floodwater; depth of floodwater; combination of velocity and depth of floodwater; isolation during a flood; effective warning time; and rate of rise of flood. However, many studies consider the development of hazard maps that use only water depth but do not consider water flow velocity (Koks et al., 2015; Sampson et al., 2015; Bates et al., 2018). While New South Wales Government (2005) highlights the importance of considering varying hazard level for flood of different severities, it does not account for different return periods to the flood hazard mapping. This situation might cause confusion among scientists, engineers or managers that use flood hazard maps which cannot be compared or used in a pre-established hazard management methodology.

Though the return period is used to identify the hazard probability, the criterion which determines the relation between the return period and the probability levels on flood hazard mapping remains arbitrary (e.g. Foudi et al., 2015). The choice of the return periods for the hazard map should consider the hydrological processes as well as the social response to them. In urban areas, the drainage system can be defined as minor drainage system, when it serves as the surface drainage system, and the major drainage system, when it serves to major flood control system (Urbonas & Roesner, 1993). For minor drainage system design, the return period of 2- or 5-year is used. For major drainage system, it is considered 100-year return period, although sometimes 10-, 25- or 50-year can be considered. It is common to observe project guidelines in which the consequences of structure failure are calculated according to the Annual Exceedance Probability (AEP) of peak-flows, however, it can lead to design mistakes due to a misunderstanding of flood risk.

The present study highlights the importance of return period choice on flood hazard degree and flood hydraulic characteristics. We combine a hydrological and a hydrodynamic model based on the methodology proposed by Monteiro & Kobiyama (2013 and 2014) to define the flood hazard intensity and flood hazard degree. The UFSC campus basin, which has a history of flood-related disasters, was used as a test bed for the study.

MATERIAL AND METHODS

Flood Hazard Index and degree

Foster & Cox (1973) were the first to research at laboratory level children's safety in floodways and the flood-related stability of people. After that, Cox et al. (2010) reviewed previous investigations that made experimental tests of people instabilities, for example, Foster & Cox (1973), Abt et al. (1989), Karvonen et al. (2000) and Jonkman & Penning-Rowsell (2008). Some new laboratory-investigations on flood-related people stability were made by Xia et al. (2014) and Martínez-Gomariz et al. (2016). Some analytical (Milanesi et al., 2015; Simões et al., 2016) and numerical (Arrighi et al., 2017) investigations about this issue. All these studies created a better comprehension of flow hazard effects and helped to define and confirm the flood hazard curves created by Smith et al. (2014).

During a flood event, the instability of pedestrians is an important subject that should not be omitted in flood hazard evaluation. The Flood Hazard Index (*HI*) can be calculated as:

$$HI = d.v \tag{1}$$

where d is the flow depth (m) and v is the flow velocity (m s^{-1}). Equation 1 is used to quantify the hazard of a flow level (Loat & Petrascheck, 1997; Stephenson, 2002; Monteiro & Kobiyama, 2013; Mani et al., 2014). Even if other formulations can be found in the literature, for example, Foudi et al. (2015) ($HI_F = d\,(v + 0.5) + df$, where df is the debris factor), *HI* in Equation 1 has an interesting and important simplicity that allows the consideration of people instability and vulnerability with only velocity and depth evaluation. Since *HI* is also used to quantify the hazard for vehicles (Xia et al., 2011; Shand et al., 2011) and buildings (Mason et al., 2012), this index is simple, practical and flexible to be used in flood hazard mapping, but have limitation on the use to represent flows with high density of fluid, such as muddy flows.

Considering the flood hazard curves (Smith et al., 2014) we can quantify and discretize the hazard intensity (Figure 1). To estimate the hazard, it is also necessary to recognize the flood probability. Some hazard maps are made using only the 100-year return period (Smith et al., 2014; Sampson et al., 2015; Bates et al., 2018) which has the short come of hindering the possibility to apply some risk assessment strategies like the Expected Annual Damage (Foudi et al., 2015). A flood hazard map should also have the information of the high-frequency hazard that, in many cases, is more useful than the low-frequency hazard.

To map the flood hazard, Loat & Petrascheck (1997) described a relation of the flood intensity with the occurrence probability related to the return period of the event obtaining hazard degrees (Table 1, Figure 2). For this evaluation, we considered all buildings as being made of concrete with solid masonry in-fill walls (Smith et al., 2014). If some structure is made of wood or another

Table 1. Description of different hazard degrees.

Hazard degree	Zone	Description
High	Red	People are in danger inside buildings because buildings can be suddenly destroyed. People outside buildings are in danger.
Medium	Orange	People are in danger outside buildings and buildings can suffer damage. Children and vehicle outside buildings are in danger.
Low	Yellow	Safe to adults, but children and vehicles can be in danger and small loss inside buildings can occur. In a low probability, it also can be a danger to adults and cause damage to buildings.

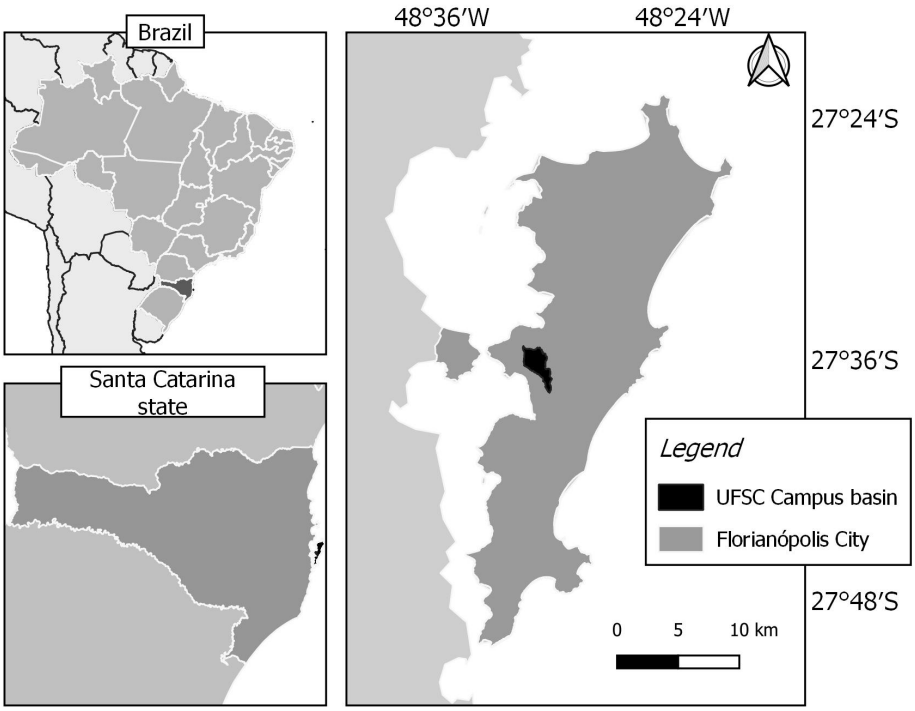

Figure 1. Hazard Intensity Curves and degree of intensity. Note that A, B, and C are the strong, medium, and weak intensity, respectively (Modified from Smith et al., 2014).

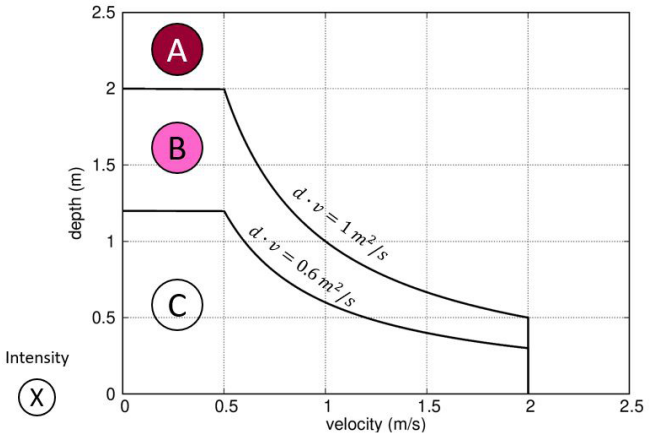

Figure 2. Intensity-Probability Diagram used to define classes of Hazard Degree (Modified from Loat & Petrascheck, 1997).

weaker material, the intensity degrees should be adjusted. Each hazard degree indicates how flood can affect people. An event with high frequency occurrence has a hazard degree increased to indicate an imminent danger of the flooded area. In this way, even if a medium intensity degree is defined, we can obtain a high hazard degree if the event has a high frequency occurrence. Werren et al. (2016) chose specific probability thresholds, according to the local practice of flood risk mitigation.

The diagram presented by the Swiss Guidelines (Loat & Petrascheck, 1997) has a dual classification on some discretisation and its classification must be chosen by the manager. Our discretisation was based on other studies in South America (i.e., García et al., 2004; García-Martínez & López, 2005; Monteiro & Kobiyama, 2013; Cabrera & Castillo, 2016) and is more severe in high frequency events and less severe in medium and low frequency events (Figure 3), delimiting zones with higher hazard degree that must be managed.

Combining the v and d values, we obtain the hazard intensity, and with the hazard intensity of three event of different probability of occurrence we get the hazard degree (Figure 3). Here we consider flood hazard map and flood hazard degree map as synonymies since hazard is the relationship between flood intensity and flood occurrence probability. One can obtain flood hazard maps using hydrological-hydrodynamic models to estimate the probability of a flood event related to the occurrence probability of a design rainfall.

The UFSC basin study area

The study area is a small and urban basin (4.09 km²), located at the Universidade Federal de Santa Catarina (UFSC), is called UFSC Campus Basin (UFSCCB). It is a part of the Itacorubi basin (25 km²), located in Florianópolis city (420,299 inhabitants), southern Brazil (Figure 4). The Itacorubi basin is the second largest one in Florianópolis city, southern Brazil, and has a history of flood-related disasters. The disordered occupation disregarding the natural aspects has been reducing the time of concentration in the basin. Additionally, the drainage system has been underdesigned and poorly maintained, contributing to the occurrence of floods (Kobiyama et al., 2006).

According to Köppen classification, the climate is Cfa, i.e., subtropical constantly humid, with hot summers and without dry season (Alvares et al., 2013). The total annual rainfall is around 1500 mm, with 140 to 158 rainy days per year (Thomé et al., 1999).

UFSCCB's main channel, called Meio river, is 4.0 km long with a mean slope of 0.09 m/m, running from South to North. The headwater sources in the basin are at about 360 m altitude and its outlet at 3-m altitude, draining into mangrove areas. The vegetation cover of the Itacorubi basin predominantly consists of secondary vegetation, but there are still remnants of the Ombrophilous Dense Forest (Atlantic Forest) in the highest parts of the basin. The land-use of UFSCCB is represented by: 39.5% of constructed area; 26.2% of sparse vegetation (small and large shrub); 16.9% of open spaces (grasses); 11.7% of dense vegetation typically characterized by a closed cover, strata formed by vegetation with an average height of 5 to 12 m, and 5.7% of exposed soil (coverless soil).

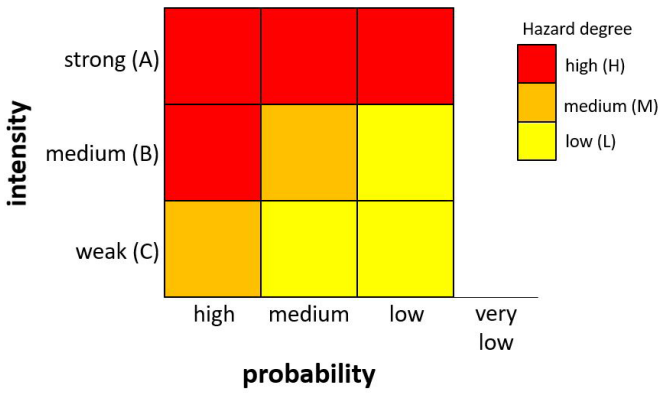

Figure 3. Flood Hazard Mapping process flowchart for different occurrence probability events.

Hydrological model application

UFSCCB has eight contributing sub-basins with different sizes, land covers and topographic characteristics (Figure 5). The hydrological model is applied on the sub-basins and the hydrodynamic model is applied in the university campus area for which the flood hazard map is created. The hydrologic models were calibrated and validated with observed hydrographs based on a return period and rainfall duration. The flood extent and hazard degree were evaluated for each contributing sub-basin.

Three steps were taken for building the rainfall-runoff hydrological model: (i) the digital filter of Eckhardt (2005) to define the base-flow; (ii) the Curve Number to define the rainfall excess distribution; and (iii) the synthetic hydrograph of NCRS (Natural Resources Conservation Service, 2007) to define the hydrograph shape. This model combination can represent flood events and we assumed that evapotranspiration could be neglected. Subsequently, the parameters found for the calibration and validation were regionalized to each contributing sub-basin.

The digital filter of Eckhardt (2005) was applied to determine the base-flow:

$$Qb_i = \frac{(1-BFI)\cdot a\cdot Qb_{i-1} + (1-a)\cdot BFI\cdot Q_i}{1-a\cdot BFI} \quad (2)$$

where Qb is the base flow ($m^3\ s^{-1}$); Q is the total runoff ($m^3\ s^{-1}$); BFI is the maximum base flow index; and a is the exponential decay in the recession period. The filter was calibrated by visual inspection, paying special attention to the inflexion points. The values of the calibrated parameters were $a = 0.995$ and $BFI = 0.80$.

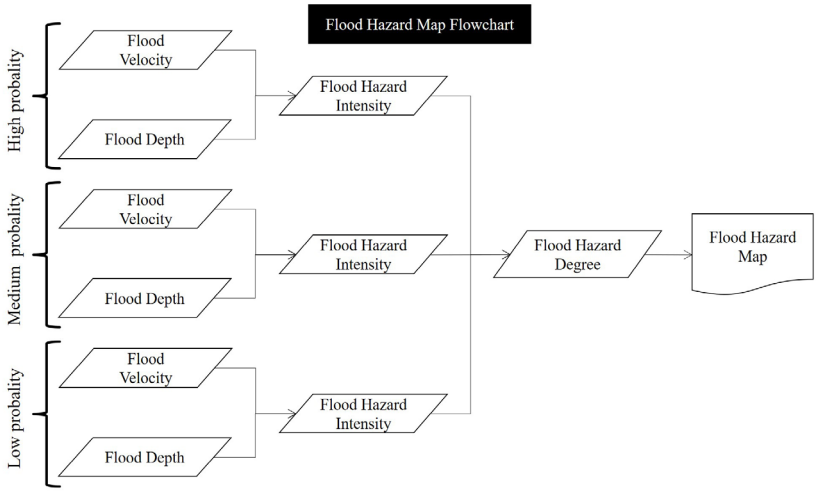

Figure 4. The locality of UFSC Campus basin.

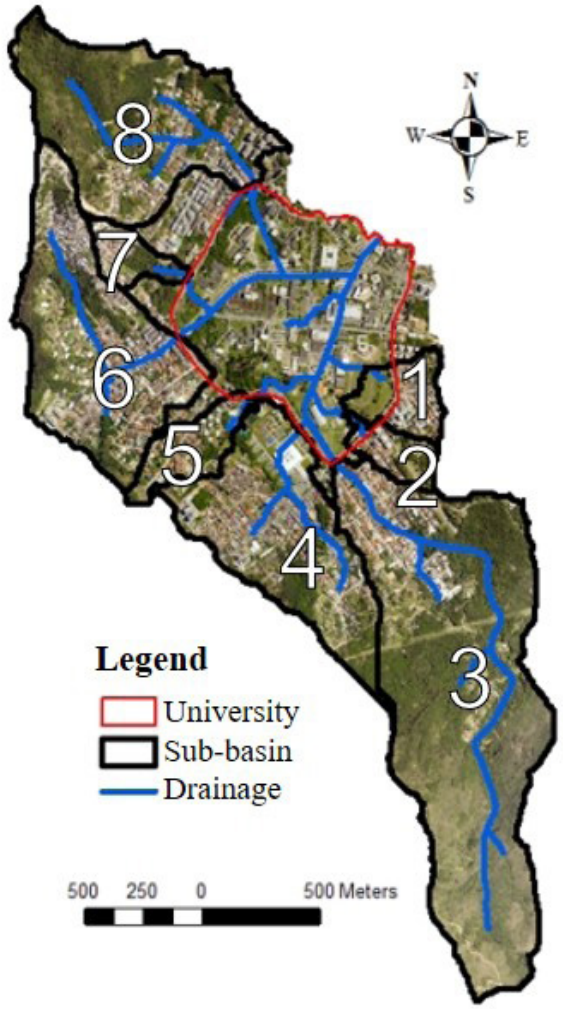

Figure 5. Aerial image of the UFSC Campus basin and eight contributing sub-basins.

To calculate base flow on validation procedure, the Eckhardt (2005) filter was modified by considering the total flow equal to the surface flow at time *i*, and the base flow at the previous moment, as:

$$Qb_i = \frac{(1-BFI)\cdot a\cdot Qb_{i-1} + (1-a)\cdot BFI\cdot (Qb_{i-1}+Qs_i)}{1-a\cdot BFI} \quad (3)$$

where Qs is the storm hydrograph ordinate ($m^3\ s^{-1}$). The volume of surface runoff was defined by using numerical integration with a trapezoidal rule:

$$V = \sum_{i=2}^{n} \Delta t \frac{(Q_i - Qb_i)(Q_{i-1} - Qb_{i-1})}{2} \quad (4)$$

where V is the surface runoff volume (m^3); and Δt is the temporal discretisation (s).

We used the SCS method (Natural Resources Conservation Service, 1986) to determine the rainfall excess distribution:

$$P_{ef,acu} = \begin{cases} 0, & for \quad P_{acu} \le Ia \\ \dfrac{(P_{acu}-Ia)^2}{P_{acu}-Ia+(-254+25400/CN)}, & for \quad P_{acu} > Ia \end{cases} \quad (5)$$

where Ia is the initial abstraction (mm); P_{acu} is the rainfall accumulated in the time (mm); $P_{ef,acu}$ is the rainfall excess accumulated in the time (mm); and CN is the Curve Number determined with land use.

The CN value should not be directly used for other soil types or for other regions outside the Midwest of the USA where the method was established. Thus, CN was calibrated for each rainfall event. When surface runoff was equal to zero, the rainfall excess was considered zero, determining the initial abstraction. The CN was determined by Equation 5, from the beginning of runoff generation until the end of the event..

The hydrograph shape was determined using the unit hydrograph convolution:

$$Qs_n = \sum_{i=1}^{n} P_i HU_{n-i+1} \quad (6)$$

where n is the time index of storm hydrograph; i is the time index of rainfall excess; and HU is the unit hydrograph ordinate ($m^3\ mm^{-1}\ s^{-1}$). The unit hydrograph method proposed by Mockus (1957) was used:

$$\frac{Q}{Q_p} = e^m \cdot \left(\frac{t}{t_p}\right)^m \cdot e^{-mt/t_p} \quad (7)$$

where Q is the runoff ($m^3\ s^{-1}$); Q_p is the runoff peak ($m^3\ s^{-1}$); m is the gamma equation shape factor; t is the time (min); and t_p is the peak time (min). The t_p value was calculated with the Kirpich formula by Chen et al. (2019):

$$t_c = 0.019 L^{0.77} S^{-0.385} \quad (8)$$

$$t_p = 0.6 t_c \quad (9)$$

where t_c is the time of concentration (min); L is the main channel length (m); and S is the main channel slope (m m^{-1}). The relationship between t_c and t_p is indicated in NRCS (Natural Resources Conservation Service, 2010).

The simplex search method proposed by Lagarias et al. (1998) was used to calibrate the model. The objective function was the absolute error of the peak time (OF):

$$OF = abs(t_{po} - t_{ps}) \quad (10)$$

where t_{po} and t_{ps} are the observed and simulated values of the peak time, respectively. The gamma equation shape (m) was the calibrated variable.

To calibrate and validate the hydrological model, UFSCCB was considered as just one basin because the outlet is the only recording gauge. Two rainfall events with a total rainfall of 13.0 mm (March 4, 2006) and 14.8 mm (March 2, 2006) were used for calibration and validation, respectively. The time interval for monitoring was 1 minute. The calibrated m value was 5.38, equivalent to a peak rate factor of 588, higher than that indicated by the NRCS (Natural Resources Conservation Service, 2007) of 484. After the model validation, we regionalized the parameters for each contributing sub-basin.

Hydrodynamic model application

An intensive rainfall that triggered a flood on January 11, 2018, was monitored and points with water presence were photographed and registered just after the event. The rainfall was registered with a time interval of 5 min. The discharge measurement gauge was not working during this event.

The HEC-RAS 5.0.5 (U. S. Army Corps of Engineers, 2016) 2D hydrodynamic model was used to route the flood wave. A new topographical model was developed using information from the Sustainable Development Secretary of Santa Catarina State (SDS/SC). A Digital Terrain Model (DTM) (1 m × 1 m) was used, and a Digital Elevation Model (DEM) (1 m × 1 m) was overlaid on buildings' places to consider their height. Both digital models have vertical accuracy of 0.39 m. Bathymetry was not added since river depth in a dry day has only a few centimeters.

Hydraulic structures such as culvert and bridges were measured on the field and added into the HEC-RAS 2D model using the SA/2D Area Connection Tool. Grids of 10 m × 10 m were generated, and break lines were added near the river path to create smaller and adjusted grids in these locations to have better fitness on the river section. A constant Manning coefficient of 0.06 was adopted, that is an intermediary value of urban developed spaces (Liu et al., 2018). Based on the Courant number, the Full Momentum equation was used with the Adjusted Time Step Tool with varied time step from 0.13 s to 8.53 min. Hydrographs obtained from the hydrological model for all the sub-basins were used as input data to 2D hydrodynamic model. A normal depth condition with slope of 0.0001 m/m was applied as the outlet boundary condition, estimated by water level variation from the DEM. To validate the flood map, 14 points obtained in the field survey after the flood event were used. Since the field survey could not be accurately map flood depth, these points represent only the presence of the flood during the event.

Flood hazard mapping

To determine rainfall quantity and intensity, the Intensity-Duration-Frequency equation for Florianópolis city (Back et al., 2011), was used:

$$i = \frac{222.0T^{0.1648}}{t^{0.3835}} \quad (11)$$

where i is the intensity (mm h^{-1}); T is the return period (year); and t is the rainfall duration (min). To determine the temporal distribution of this precipitation, the fourth quartile proposed by Huff (1967) was adopted. Monteiro & Kobiyama (2014) demonstrated that the fourth quartile generates the largest flood area and the highest hydrograph peak. According to Innocente et al. (2018), the critical rainfall duration that provides the largest hydrograph volume and peak for any return period of UFSCCB is 110 minutes which was adopted for the model application to create the hazard flood map, but not for calibration and validation. Since UFSCCB area is relatively small, the same rainfall duration is used for each sub-catchment.

The rainfall events were designed with the return periods of 2, 10, 25, 50, 100 and 500 years. For each return period, the rainfall-runoff model was used to simulate hydrographs for all the contributing sub-basins.

Flood events were simulated with the validated hydrodynamic model and as inlet boundary condition hydrographs for each T value were applied. We considered the hazard intensity and hazard degree, proposed in Figure 2 and Figure 3, to obtain the flood hazard maps.

RESULTS AND DISCUSSIONS

Hydrological and hydrodynamic models' performances

The calibrated and validated events are shown in Figure 6. The data time step was of 1 min, and the *OF* values for calibration and validation are 2.9 min and 0.4 min, respectively, showing a good peak time adherence of the model. Note that *OF* value can be smaller than the time step since we have a continuous function to represent the unit hydrograph. Visual analysis permits to recognize that both events are well represented.

After the validation of the hydrological model, the parameters for each contributing sub-basin were regionalized. The Eckhardt

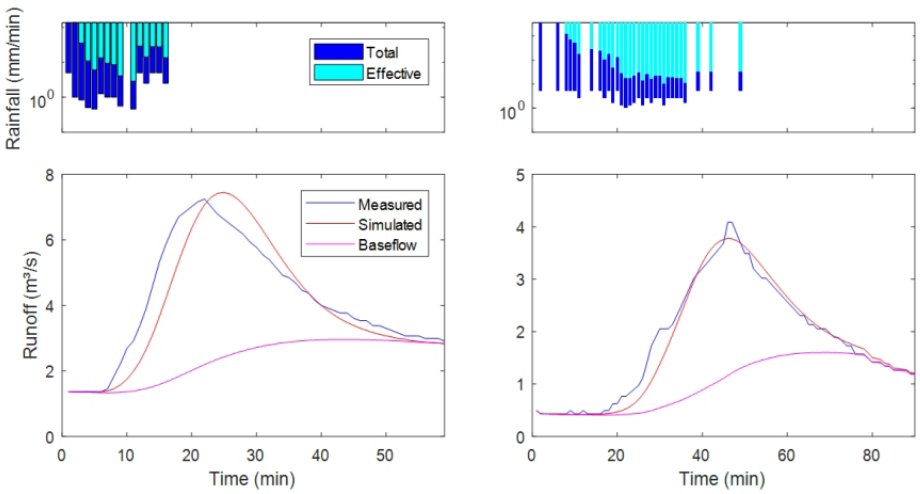

Figure 6. Hyetographs and hydrographs of hydrological model calibration (left) for the event (04MAR2006) and validation (right) for the event (02MAR2006).

filter parameters for baseflow were considered constant for all the sub-basins. To estimate the unit hydrograph, we used the constant *m* value for all sub-basins, but we varied the *tp* based on Equations 8 and 9 for each sub-basin.

The *CN* value was determined for each contributing sub-basin using image classification, in which three classes were considered: i) residential areas 1/8 Acre lots, about 65% impervious (*CN* = 80); ii) open spaces in good conditions, with grass cover more than 75% of area (*CN* = 65) and iii) woods and forests good conditions with 50-75% ground cover, not heavily grazed (*CN* = 55). To determine the value of each class of *CN*, values close to those presented in NRCS (Natural Resources Conservation Service, 1986) were sought in which the weighted average per area resulted in the calibrated *CN* value for the UFSCCB basin. The initial abstraction parameter for each subbasin was calibrated as a fixed percentage of the storage capacity. Calculated and regionalized values are shown in Table 2.

Using these hydrographs, the flood event was simulated with the hydrodynamic model and compared with observed points (Figure 7). Points inside flooded areas and near flood boundary considering half of the simulation mesh (respecting the sensibility of considered mesh), i.e., 5 m, were considered to be well represented by the model (Figure 8). Among 14 points, 12 were correctly represented, and the other two have both 8-m distance from the simulated flood event. Between the 12 points correctly evaluated flood maximum velocity varied from 0.05 to 0.90 m/s.

Analysis of the hazard intensity and degree

Flood intensity maps for each *T* value were generated (Figure 9). Table 3 shows the values of rainfall intensity, rainfall volume, flood flow velocity, flood depth, flood area and intensity extent (IE) for strong, medium and weak intensity for each return period. It should be noted that rainfall intensity and volume depend only on *T* meanwhile flood characteristics depend on hyetograph shape and basin characteristics.

The maximum-depth location changes depending on *T*. In case of *T*=2-years flood event, the maximum-depth location is

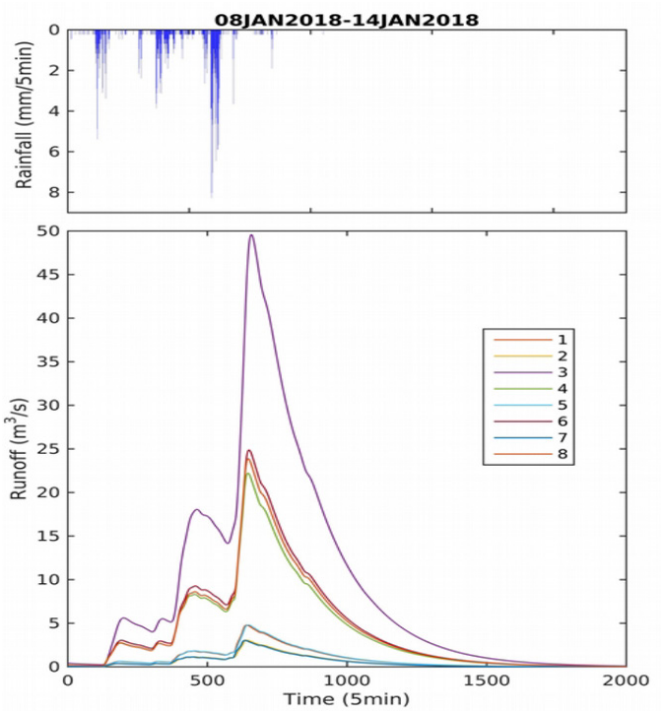

Figure 7. Observed hyetograph and simulated hydrograph of January 2018 flood event for all the sub-basins 1 to 8.

Table 2. Calculated and regionalized parameters of hydrological model for 8 contributing sub-basins.

Sub-basin	*L* (km)	*S* (%)	*tp* (min)	Area (km²)	*CN*	*Ia* (mm)
UFSCCB	3.83	9.27	16.35	4.08	64.69	0.65
1	0.38	2.35	10.31	0.10	67.97	0.68
2	0.46	2.60	11.28	0.07	67.50	0.68
3	2.74	12.69	21.28	1.19	61.48	0.61
4	1.15	9.67	13.32	0.49	66.89	0.67
5	0.72	3.27	13.96	0.11	67.91	0.68
6	1.36	7.78	15.89	0.56	65.61	0.66
7	0.46	19.20	5.95	0.07	66.67	0.67
8	1.36	11.48	14.03	0.56	62.14	0.62

Table 3. Variables values for different return periods.

Return Period (year)	2	10	25	50	100	500	Rate (500/2)
Rainfall Intensity (mm h⁻¹)	41.02	53.49	62.21	69.74	78.18	101.92	2.48
Rainfall Volume (m³)	6,759	10,278	12,974	15,428	18,293	26,865	3.97
Flood Maximum Depth (m)	3.79	4.10	4.25	4.38	4.46	5.11	1.35
Flood Average Depth (m)	1.11	1.27	1.34	1.36	1.39	1.47	1.32
Flood Maximum Velocity (m s⁻¹)	1.98	2.48	2.62	2.71	2.79	3.09	1.56
Flood Average Velocity (m s⁻¹)	0.38	0.40	0.41	0.43	0.45	0.53	1.39
Flood Area (m²)	92,534	111,849	127,228	142,746	155,054	179,575	1.94
Weak IE (m²)	72,482	77,247	82,807	90,900	96,411	102,043	1,41
Medium IE (m²)	4,235	6,269	6,784	7,184	7,801	11,385	2.69
Strong IE (m²)	15,817	28,333	37,637	44,662	50,842	66,147	4.18

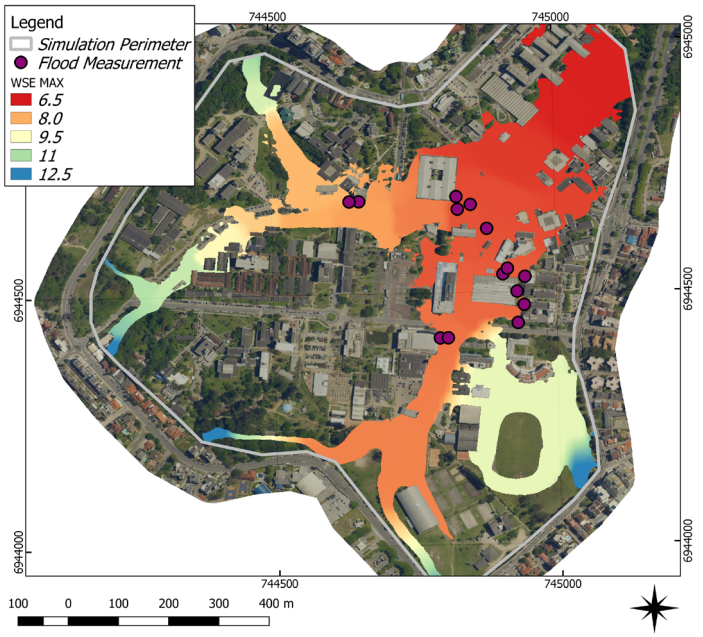

Figure 8. Simulated flood area and measured points of JAN2018 event.

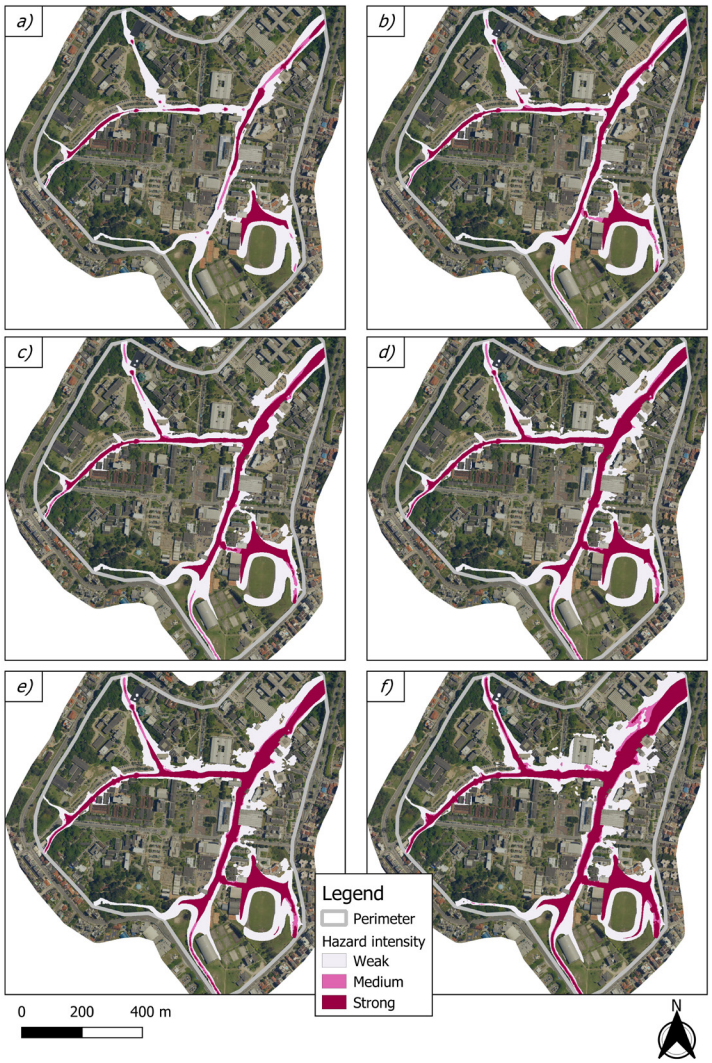

Figure 9. Flood Intensity maps for different return periods: (a) 2 years, (b) 10 years, (c) 25 years, (d) 50 years, (e) 100 years and (f) 500 years.

Table 4. Logarithm formula of variables to the return period (*T*).

	Formula	R2
Rainfall Intensity (mm.h^{-1})	= 10.95ln(*T*) + 29.53	0.98
Rainfall Volume (m^3)	= 3602ln(*T*) + 2524	0.96
Flood Maximum Depth (m)	= 0.226ln(*T*) + 3.560	0.95
Flood Mean Depth (m)	= 0.063ln(*T*) + 1.103	0.95
Flood Maximum Velocity (m.s^{-1})	= 0.191ln(*T*) + 1.945	0.96
Flood Mean Velocity (m.s^{-1})	= 0.026ln(*T*) + 0.342	0.88
Flood Area (m^2)	= 0.023ln(*T*) + 0.110	0.99
Weak-IE (m^2)	= 0.008ln(*T*) + 0.094	0.96
Medium-IE (m^2)	= 0.013ln(*T*) + 0.012	1.00
Strong-IE (m^2)	= 0.002ln(*T*) + 0.004	0.93

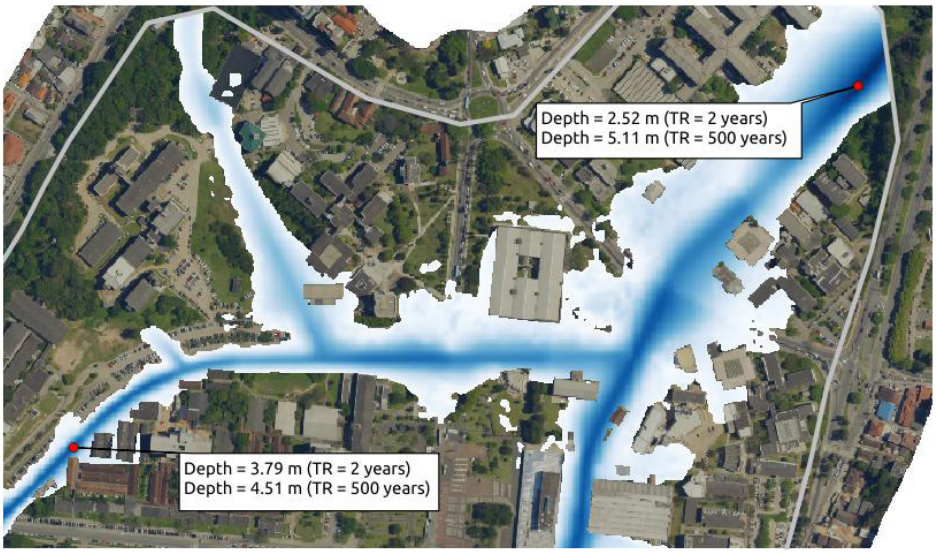

Figure 10. Maximum depth at two points for the 2-year and 500-year return periods.

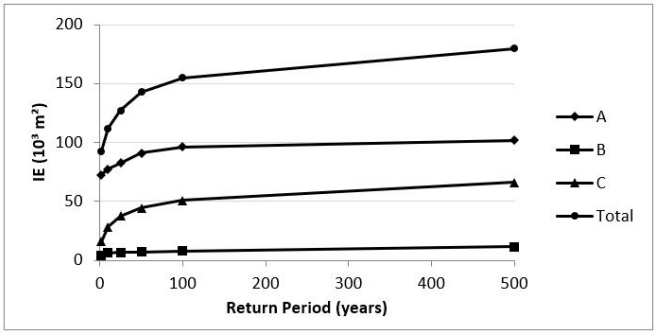

Figure 11. Hazard IE with different return periods. Note that A, B, and C are strong, medium, and weak-intensity degree, respectively.

on the river upstream in a small tributary (just after the confluence between the sub-basin 6 and 7) meanwhile for the *T*=500-years flood event it is on the river downstream near outlet boundary condition (Figure 10).

Strong hazard intensity increases more quickly with the increase in *T* than medium and weak hazard intensity, but all the IE values always increase (Figure 11). Each area does not change largely with *T* over 100 years. The strong-IE increased in 4.18 times (Table 3) from the 2- to 500-year return period meanwhile, the weak-IE in 1.41 times. For all values of *T* the largest IE is always the weak one.

All the variables presented in Table 3 can be expressed by the logarithm formulation (Table 4). Figure 11 and Table 4 imply that in the UFSCCB the geomorphic feature changes more expressively for the smaller *T* values. In other words, the hydrological response of sub-basins and the channel network regions (flood areas) are more sensitive to the short *T* till 100 years.

The hazard map (i.e. flood hazard degree map) considers different flood hazard intensities (Figure 9). According to Loat & Petrascheck (1997), at least three values of *T* must be used (Table 5). The hazard degree is related to which urban system is analyzed: (i) low hazard degree should be ensured by minor drainage systems; (ii) medium hazard degree should be ensured by major drainage system, since the minor drainage system will probably fail; and (iii) high hazard degree are related to buildings security since the buildings usually have more resistance to medium and low hazard degree. We have eight possible combinations to construct the flood hazard map based on Table 5. Two classes that represent the extreme situations were analyzed: the weakest hazard map with the 2-, 25-, 100-year return period; and the strongest hazard map with the 10-, 50- and 500-year return period (Figure 12).

For flood mitigation measures, we could consider the football field as a floodwater storage system as suggested in the literature (e.g.,

Table 5. Probability characteristics of flood hazard map.

Hazard Degree	Return Periods (year)	Characteristics
Low	2 or 10	Minor drainage system
Medium	25 or 50	Major drainage system
High	100 or 500	Buildings security

Table 6. Hazard degree area variation.

Hazard degree	Weakest scenario (m^2)	Strongest scenario (m^2)	Difference (m^2)	Relative Difference (%)
Low	62,226	66,729	4,503	7.2
Medium	41,986	46,680	4,694	11.2
High	50,842	66,166	15,324	30.1
Total	155,054	179,575	24,521	15.8

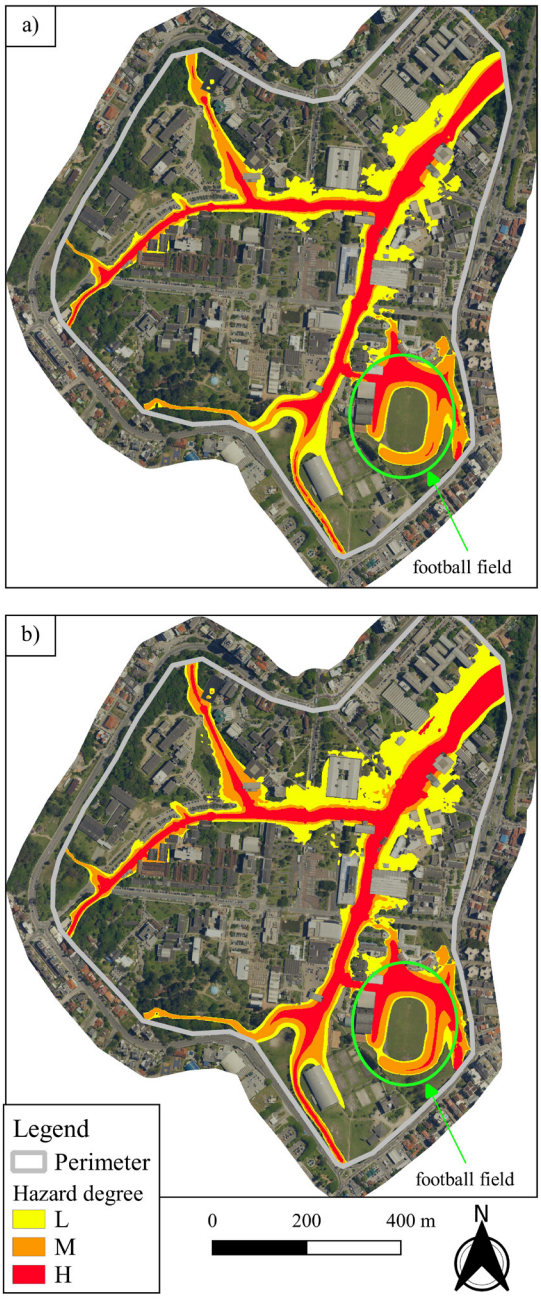

Figure 12. Flood Hazard maps: (a) the highest recurrence scenario (weakest hazard); and (b) the lowest recurrence scenario (strongest hazard).

Yamashita et al., 2013); however, its surrounding area is only inundated with the Medium and High hazard degree. We suggest that bigger storage areas' effects on flood must be analyzed with the strongest hazard scenario to verify which buildings can still be in danger.

Small storage areas, like parking lots, should be analyzed with the weakest hazard map since it will affect people on the pathways (Martínez-Gomariz et al., 2016) and cars (Ball et al. 2019), and a more frequent hazard is important. Pathways covered by any flood hazard degree should be notified to local people even at the disaster prevention stage (or pre-event stage). To provide safety we encourage that storage areas must have warnings or/and alert system.

There is a difference of about 16% of the total area between the two situations and the high hazard degree changed by 30% (Table 6). However, even with this variation, there is no difference between the numbers of buildings affected by medium and high hazard degree. This comparison also shows that the high hazard degree area is most sensitive to the return period selection, which indicates the buildings safety.

CONCLUSIONS

In this study, we defined the flood hazard intensity and flood hazard degree and showed their importance on hazard assessment. We found that in the case of UFSCCB, the small variation of flood average velocity indicates that storage areas are significant even for 500-years event and these areas should be part of the major drainage system. We elaborated two flood hazard maps, a low hazard one that that combines 2-, 25-, 100-years return periods and a high hazard one that combines the 10-, 50- and 500-years return period. The comparison of hazard maps between the two scenarios shows that the high hazard degree area is the most sensitive to the return period selection.

Return period (T) has a double effect on flood hazard mapping. The first effect is that T, as probability, will compose hazard degree. The second effect is that rainfall level increases with T and, consequently, velocity and flow depth change according to the river channel and floodplain characteristics. Therefore, we argue that flood managers should consider return period carefully since it can cause important changes on a hazard mapping, mainly on high hazard zones.

These results can support flood management as they provide a framework for understanding the flood variables related to return period that are relevant for flood hazard mapping. Some important considerations should be made in further development of this methodology for flood risk mapping, such as other flood variables (e.g., duration and the rate of rise of floodwaters) and societal vulnerability.

ACKNOWLEDGEMENTS

Dr Ron Cox (Associate Professor of UNSW Water Research Laboratory) is thanked for providing useful information on people and vehicle stability.

REFERENCES

Abt, S., Wittier, R., Taylor, A., & Love, D. (1989). Human stability in a high flood hazard zone. *Journal of the American Water Resources Association*, *25*(4), 881-890. http://dx.doi.org/10.1111/j.1752-1688.1989.tb05404.x.

Alvares, C. A., Stape, J. L., Sentelhas, P. C., de Moraes Gonçalves, J. L., & Sparovek, G. (2013). Köppen's climate classification map for Brazil. *Meteorologische Zeitschrift (Berlin)*, *22*(6), 711-728. http://dx.doi.org/10.1127/0941-2948/2013/0507.

Arrighi, C., Oumeraci, H., & Castelli, F. (2017). Hydrodynamics of pedestrians' instability in floodwaters. *Hydrology and Earth System Sciences*, *21*(1), 515-531. http://dx.doi.org/10.5194/hess-21-515-2017.

Back, A. J., Henn, A., & Oliveira, J. L. R. (2011). Heavy rainfall equations for Santa Catarina, Brazil. *Revista Brasileira de Ciência do Solo*, *35*(6), 2127-2134. http://dx.doi.org/10.1590/S0100-06832011000600027.

Ball, J., Babister, M., Nathan, R., Weeks, W., Weinmann, E., Retallick, M., & Testoni, I. (Eds.), (2019). *Australian rainfall and runoff: a guide to flood estimation*. Commonwealth of Australia: Geoscience Australia.

Bates, P.D., Neal, J., Sampson, C., Smith, A., & Trigg, M., (2018). Progress toward hyper resolution models of global flood hazard. In G. Michel. *Risk modeling for hazards and disasters* (pp. 211-232). USA: Elsevier. https://doi.org/10.1016/C2015-0-01065-6.

Cabrera, C. J., & Castillo, N. L. (2016). Evaluation of flexible barrier and sabo dam to control effects of debris flow in Santo Domingo Ravine. In *Hydraulic Barriers and Water System Management. 6th IAHR International Symposium on Hydraulic Barriers* (pp. 27-30). Beijing: IAHR.

Chen, Y., Shi, P., Ji, X., Qu, S., Zhao, L., & Dong, F. (2019). New method to calculate the dynamic factor–flow velocity in Geomorphologic instantaneous unit hydrograph. *Scientific Reports*, *9*(1), 14201. PMid:31578394. http://dx.doi.org/10.1038/s41598-019-50723-x.

Cox, R., Shand, T., & Blacka, M. (2010). *Australian rainfall and runoff, revision project 10: appropriate safety criteria for people* (Stage Report). Australia: Engineers Australia Water Engineering.

Eckhardt, K. (2005). How to construct recursive digital filters for baseflow separation. *Hydrological Processes: An International Journal*, *19*(2), 507-515. http://dx.doi.org/10.1002/hyp.5675.

Foster, D., & Cox, R. (1973). *Stability of children on roads used as floodways: preliminary study* (Technical report). Sydney, Austrália: Water Research Laboratory, University of New South Wales.

Foudi, S., Osés-Eraso, N., & Tamayo, I. (2015). Integrated spatial flood risk assessment: the case of Zaragoza. *Land Use Policy*, *42*, 278-292. http://dx.doi.org/10.1016/j.landusepol.2014.08.002.

García, R., Rodríguez, J. J., & O'Brien, J. S. (2004). Hazard zone delineation for urbanized alluvial fans. In D. K. Stevens, G. Sehlke, & D. F. Hayes (Eds.), *Critical transitions in water and environmental resources management* (pp. 1-10). Reston: Amer Society of Civil Engineers. http://dx.doi.org/10.1061/40737(2004)11.

García-Martínez, R., & López, J. L. (2005) Debris flows of December 1999 in Venezuela. In M. Jakob & O. Hungr. *Debris-flow hazards and related phenomena*. Berlin, Heidelberg: Springer Praxis Books. http://dx.doi.org/10.1007/3-540-27129-5_20.

Huff, F. A. (1967). Time distribution of rainfall in heavy storms. *Water Resources Research*, *3*(4), 1007-1019. http://dx.doi.org/10.1029/WR003i004p01007.

Innocente, C., Monteiro, L. R., Corseuil, C. W., Kobiyama, M., & Chaffe, P. L. B. (2018). Um estudo sobre a definição da duração crítica da chuva de projeto na bacia da UFSC, Florianópolis- SC. In *Anais do I Encontro Nacional de Desastres*. Associação Brasileira de Recursos Hídricos, 1-8.

Jonkman, S., & Penning-Rowsell, E. (2008). Human instability in flood flows. *Journal of the American Water Resources Association*, *44*(5), 1208-1218. http://dx.doi.org/10.1111/j.1752-1688.2008.00217.x.

Karvonen, R., Hepojoki, A., Huhta, H., & Louhio, A. (2000). *The use of physical models in dam-break flood analysis*. Finland: Helsinki University of Technology.

Kobiyama, M., Grison, F., Lino, J. F., & Silva, R. V. (2006). Time of concentration in the UFSC campus catchment, Florianópolis-SC (Brazil), calculated with morphometric and hydrological methods. In *Anais do VI Simpósio Nacional de Geomomorfologia e Regional* (pp. 1-11). Goiânia: Universidade Federal de Goiás.

Koks, E. E., Jongman, B., Husby, T. G., & Botzen, W. J. (2015). Combining hazard, exposure and social vulnerability to provide lessons for flood risk management. *Environmental Science & Policy*, *47*, 42-52. http://dx.doi.org/10.1016/j.envsci.2014.10.013.

Lagarias, J. C., Reeds, J. A., Wright, M. H., & Wright, P. E. (1998). Convergence properties of the nelder–mead simplex method in low dimensions. *SIAM Journal on Optimization*, *9*(1), 112-147. http://dx.doi.org/10.1137/S1052623496303470.

Liu, Z., Merwade, V., & Jafarzadegan, K. (2018). Investigating the role of model structure and surface roughness in generating flood inundation extents using one- and two-dimensional hydraulics models. *Journal of Flood Risk Management*, *12*(1), e12347. http://dx.doi.org/10.1111/jfr3.12347.

Loat, R., & Petrascheck, A., (1997). *Prise en compte des dangers dus aux crues dans le cadre des activités de l´aménagement du Territoire*. Bienne: Office Fédéral de l´Economie des Eaux (OFEE), Office Fédéral de l´aménagement

du Territoire (OFAT), Office Fédéral de l´Environnement, des Forêts et du Paysage (OFEFP).

Mani, P., Chatterjee, C., & Kumar, R. (2014). Flood hazard assessment with multiparameter approach derived from coupled 1d and 2d hydrodynamic flow model. *Natural Hazards*, *70*(2), 1553-1574. http://dx.doi.org/10.1007/s11069-013-0891-8.

Martínez-Gomariz, E., Gómez, M., & Russo, B. (2016). Experimental study of the stability of pedestrians exposed to urban pluvial flooding. *Natural Hazards*, *82*(2), 1259-1278. http://dx.doi.org/10.1007/s11069-016-2242-z.

Mason, M. S., Phillips, E., Okada, T., & O'Brien, J. (2012). *Analysis of damage to buildings following the 2010–11 eastern Australia floods.* Australia: National Climate Change Adaptation Research Facility.

Milanesi, L., Pilotti, M., & Ranzi, R. (2015). A conceptual model of people's vulnerability to floods. *Water Resources Research*, *51*(1), 182-197. http://dx.doi.org/10.1002/2014WR016172.

Mockus, V. (1957). *Use of storm and watershed characteristics in synthetic hydrograph analysis and application*. Latham, MD: US Department of Agriculture, Soil Conservation Service.

Monteiro, L. R., & Kobiyama, M. (2013). Proposta de metodologia de mapeamento de perigo de inundação. *Revista de Gestão de Águas da América Latina*, *10*(2), 13-25. http://dx.doi.org/10.21168/rega.v10n2.p13-25.

Monteiro, L. R., & Kobiyama, M. (2014). Influências da distribuição temporal de precipitação no mapeamento de inundação. *Revista de Gestão de Águas da América Latina*, *11*(2), 25-35. http://dx.doi.org/10.21168/rega.v11n2.p25-35.

Najibi, N., & Devineni, N. (2018). Recent trends in the frequency and duration of global floods. *Earth System Dynamics*, *9*(2), 757-783. http://dx.doi.org/10.5194/esd-9-757-2018.

Natural Resources Conservation Service – NRCS, & United States Department of Agriculture – USDA. (1986). *Urban hydrology for small watersheds*. Washington: NRCS/USDA.

Natural Resources Conservation Service – NRCS, & United States Department of Agriculture – USDA. (2007). *Hydrology national engineering handbook – part 630 hydrology*. Washington: NRCS/USDA.

Natural Resources Conservation Service – NRCS, & United States Department of Agriculture – USDA. (2010). Hydrographs. In: Natural Resources Conservation Service – NRCS, & United States Department of Agriculture – USDA. *National engineering handbook. hydrology* (chap. 16). Washington: NRCS/USDA.

NSW Government. (2005). *Floodplain development manual*. Sydney, Australia: Department of Infrastructure, Planning and Natural Resources.

Sampson, C. C., Smith, A. M., Bates, P. D., Neal, J. C., Alfieri, L., & Freer, J. E. (2015). A high-resolution global flood hazard model. *Water Resources Research*, *51*(9), 7358-7381. PMid:27594719. http://dx.doi.org/10.1002/2015WR016954.

Shand, T. D., Smith, G. P., Cox, R. J., Blacka, M., et al.(2011) Development of appropriate criteria for the safety and stability of persons and vehicles in floods. In *Proceedings of the 34th World Congress of the International Association for Hydro-Environment Research and Engineering: 33rd Hydrology and Water Resources Symposium and 10th Conference on Hydraulics in Water Engineering* (pp. 404). Barton: Engineers Australia.

Simões, A. L. A., Schulz, H. E., & Luz, L. D. (2016). Dimensionless formulation for human stability in open flows. *Revista Brasileira de Recursos Hídricos*, *21*(4), 666-673. http://dx.doi.org/10.1590/2318-0331.011616019.

Smith, G., Davey, E., & Cox, R. (2014). *Flood hazard* (WRL Technical Report 2014/07. Sydney: UNSW.

Speckhann, G. A., Borges Chaffe, P. L., Fabris Goerl, R., Abreu, J. J., & Altamirano Flores, J. A. (2017). Flood hazard mapping in Southern Brazil: a combination of flow frequency analysis and the HAND model. *Hydrological Sciences Journal*, *63*(1), 87-100. http://dx.doi.org/10.1080/02626667.2017.1409896.

Stephenson, D. (2002). Integrated flood plain management strategy for the Vaal. *Urban Water*, *4*(4), 423-428. http://dx.doi.org/10.1016/S1462-0758(02)00032-8.

Thomé, V.M.R., Zamprieri, S., Braga, H.J., Pandolfo, C., Silva Junior, V.P., Bacic, I., Laus Neto, J., Soldateli, D., Gebler, E., Ore, J.D., Echeverria, L., Mattos, M., & Suski, P.P. (1999). *Zoneamento agroecológico e socioeconômico de Santa Catarina*. Florianópolis: EPAGRI.

U. S. Army Corps of Engineers – USACE, & Hydrologic Engineering Center – HEC. (2016). *HEC-RAS River Analysis System Hydraulic Reference Manual, Version 5.0*. Brummer, G. W.: USACE/HEC.

Urbonas, B. R., & Roesner, L. (1993). Hydrologic design for urban drainage and flood control. In D. R. Maidment. *Handbook of hydrology*. USA: McGrawHill.

Werren, G., Reynard, E., Lane, S. N., & Balin, D. (2016). Flood hazard assessment and mapping in semi-arid piedmont areas: a case study in Beni Mellal, Morocco. *Natural Hazards*, *81*(1), 481-511. http://dx.doi.org/10.1007/s11069-015-2092-0.

Xia, J., Falconer, R. A., Guo, P., & Gu, A. (2014). Stability criterion for a flooded human body under various ground slopes. In *Proceedings of the 11th International Conference on Hydroinformatics* (pp. 17-21). New York: Curran Associates, Inc.

Xia, J., Teo, F. Y., Lin, B., & Falconer, R. A. (2011). Formula of incipient velocity for flooded vehicles. *Natural Hazards*, *58*(1), 1-14. http://dx.doi.org/10.1007/s11069-010-9639-x.

Yamashita, S., Shimatani, Y., Watanabe, R., Moriyama, T., Minagawa, T., Kakudo, K., & Yamashita, T. (2013). Comprehensive flood control

involving citizens in a Japanese watershed. *Water Science and Technology*, *68*(4), 791-798. PMid:23985508. http://dx.doi.org/10.2166/wst.2013.293.

Authors contributions

Leonardo Romero Monteiro: Conceptualization, Formal analysis, Methodology, Investigation, Writing - original draft.

Camyla Innocente dos Santos: Formal analysis, Methodology, Investigation, Writing - original draft.

Masato Kobiyama: Conceptualization, Formal analysis, Methodology, Writing - original draft.

Cláudia Weber Corseuil: Conceptualization, Writing - original draft.

Pedro Luiz Borges Chaffe: Formal analysis, Methodology.

Editor-in-Chief: Adilson Pinheiro
Associated Editor: Priscila Macedo Moura

View publication stats